RSC Advances

PAPER

View Article Online
View Journal | View Issue

Cite this: *RSC Adv.*, 2022, **12**, 16860

A novel construct of an electrochemical acetylcholinesterase biosensor for the investigation of malathion sensitivity to three different insect species using a $NiCr_2O_4$/g-C_3N_4 composite integrated pencil graphite electrode

Sehrish Bilal, [ab] Muhammad Nasir, [b] M. Mudassir Hassan,[b] Muhammad Fayyaz ur Rehman, [d] Amtul Jamil Sami*[ac] and Akhtar Hayat*[b]

Herein, an electrochemical biosensor has been prepared to assess the sensitivity of an organophosphate insecticide, malathion, to acetylcholinesterase (AChE) enzyme of three insects including *Apis mellifera* (honeybee), *Tribolium castaneum* (red flour beetle), and *Zootermopsis nevadensis* (dampwood termite). A composite of nickel chromite ($NiCr_2O_4$) and graphitic carbon nitride (g-C_3N_4) was prepared and characterized for its morphological, chemical and electrical properties. The $NiCr_2O_4$/g-C_3N_4 composite integrated pencil graphite electrodes were used to covalently immobilize insect AChE enzymes and amperometric response of bioelectrodes was determined through cyclic voltammetry. The prepared bioelectrodes exhibited high enzyme immobilization efficiency and electro-catalytic performance. The integrated bioelectrodes could efficiently detect malathion induced inhibition of insects' AChEs. The linear ranges for malathion were found to be 0.1–1.6 μM, 1–40 nM and 2–100 nM, and LODs were 2 nM, 0.86 nM and 2.3 nM for *A. mellifera*, *T. castaneum*, and *Z. nevadensis*, respectively. Additionally, the biosensing platform developed using *A. mellifera* AChE was found highly sensitive and effective for malathion recoveries from spiked wheat flour samples with high recovery rates. Moreover, the proposed method was adequately reproducible and selective. The results revealed that *A. mellifera* AChE is less sensitive to inhibition by malathion as compared to *T. castaneum*, and *Z. nevadensis* AChE. The experimental results were validated through computational docking of malathion with insect AChEs and the results were in correspondence to experimental outcomes. The proposed method can be a plausible alternate to conventional analytical methods to assess the pesticide sensitivity and toxicity of various compounds against insect enzymes.

Received 26th February 2022
Accepted 23rd May 2022

DOI: 10.1039/d2ra01307j

rsc.li/rsc-advances

1. Introduction

The control of insect infestation in agriculture is largely dependent on chemical pesticides. However, the unrestrained use of these pesticides is greatly disturbing the environment, human health, and survival of beneficial insects.[1–3] The available toxicity data of various pesticides suggest that insect and pest enzymes behave disparately in the presence of different pesticides; for instance, honeybees have been found more susceptible to some insecticides and resistant towards other chemical or bio-pesticides, whereas red flour beetles possess reduced sensitivity against chemical and organic pesticides.[4] A principle mechanism manipulated by insects or pests to resist pesticide effects is metabolic resistance. More than 500 species of insects are resistant to various classes of pesticides all over the world.[5]

Among other widely used insecticides, malathion is a wide spectrum insecticide used for more than 50 years in agriculture, industrial and outdoor house applications to control insects or ectoparasites. Malathion is a phosphate ester having low persistence in the environment and readily converts to its metabolic forms such as malaoxon, which is a potent acetylcholinesterase (AChE) inhibitor. Malathion toxicity varies from moderate to high in target and non-targeted organisms. It has been found potentially toxic to birds, fish, aquatic larvae of terrestrial insects, and bees. It has been reported that malathion residues are highly toxic to honey bees and cause serious losses

[a]*School of Biochemistry and Biotechnology, University of the Punjab, Lahore 54000, Pakistan. E-mail: sehrishbilal33@gmail.com; Tel: +92 3364318117*

[b]*Interdisciplinary Research Center in Biomedical Materials (IRCBM), COMSATS University Islamabad, Lahore Campus, Lahore 54000, Pakistan. E-mail: muhammadnasir@cuilahore.edu.pk; mudassirhassan.27@gmail.com*

[c]*Center for Biosensor Research and Development (CBRD), University of the Punjab, Lahore 54000, Pakistan. E-mail: amtuljamilsami@yahoo.com; Tel: +92 3317648259*

[d]*Institute of Chemistry, University of Sargodha, Sargodha, Sargodha 40100, Pakistan. E-mail: muhammad.fayyaz@uos.edu.pk*

in other beneficial insect populations[6,7] reported a huge loss of honeybees in apiaries due to malathion bait that was used to control mosquitos. Further this insecticide is commonly used on stored products considering its low mammalian toxicity and acute toxicity against insects such as *Tribolium castaneum* and other beetles which are highly resilient against many other insecticides that are considered suitable for food control.[8] About half of the total applications of malathion in the US are on stored crops such as wheat, rice, sorghum, cotton and alfalfa. Many insects possess enzyme systems which are responsible for the detoxification of insecticides, explaining the selective toxicity of insects towards different insecticides. Several studies have reported the role of malathion carboxylesterases in conferring resistance to some insects including *T. castaneum*.[9–12]

Most commonly, the content of pesticides is indirectly determined by monitoring the degree of inhibition of AChE activity through methods based on enzyme-inhibition. To date a wide variety of analytical methods have been devised for both qualitative and quantitative determination of AChE activity and its inhibition, including bioassays, colorimetric Ellman's assay, radioactive methods, thin layer chromatography, gas chromatography or HPLC, *etc.* Although these methods are widely used and considered quite sensitive, they offer limitations such as low specificity, being labour-intensive and hold certain ethical limitations.[13] From the past decade the use of electrochemical biosensors has emerged as sensitive and reliable tools to bridge the gap between traditional assays and newly developed techniques.[14,15] These biosensors integrate AChE as a recognition element with an electrochemical signalling platform and work by amperometric detection of electron loss associated with irreversible oxidation of thiocholine (Tch) after AChE catalysis. These biosensors can be used to investigate pesticide toxicity to enzymes and detection of pesticide residues in environmental and agricultural samples.[16–20]

The enzyme-based biosensors provide fast response and high sensitivity and when combined with an efficient transducer material offer new ways in biosensor engineering. The key factor to develop a high performance biosensor is to retain the catalytic activity of the enzyme after immobilization on the electrode surface. Moreover, the strategy for transmission of electrochemical signals should be well defined because biological elements are naturally non-conductive. An appropriate sensing electrode fabricated with a suitable modifier material can fulfil the demands of modern electrochemical technology.[21–25]

A new class of binary transition metals known as spinals, having the chemical formula AB_2O_4, have emerged as attractive materials with promising applications in physics, materials science, geophysics, *etc.* They have also been used as advanced electrode materials for efficient energy storage devices.[26] Chromites belong to normal type spinal structures, among which nickel chromite ($NiCr_2O_4$) is of significant importance due to its role in industry as an efficient catalytic material.[27–29] The spinals offer high electrochemical activity and capacity than mono metal oxides and can be used to develop potential composite materials with enhanced catalytic selectivity and efficiency.[30,31] Furthermore, the carbon based materials such as graphene have greatly improved the biosensor industry and its 2D analogue graphitic carbon nitride has replaced graphene as a new type of functional material with remarkable physiochemical properties.[32] The $NiCr_2O_4$ particles when combined with graphitic carbon nitride (g-C_3N_4) form a novel $NiCr_2O_4$/g-C_3N_4 composite material combining the catalytic, electrical, electron rich and surface functionalities of both components.

In this work, a pencil graphite electrode (PGE) modified with a $NiCr_2O_4$/g-C_3N_4 composite (referred further to as Ni/GCN) was exploited to immobilize AChE enzymes from two pests *T. castaneum* (red flour beetle) and *Z. nevadensis* (dampwood termite), and a non-target social insect *A. mellifera* (honeybee). The prepared composite was expected to possess high surface area with enhanced electrical conductivity and immobilization efficiency. Under optimized conditions, the fabricated bioelectrodes with the structure AChE/Ni/GCN/PGE were used to test the sensitivity of malathion against insect AChEs by electrochemical assay using cyclic voltammetry. The proposed structure was also applied for real time detection of malathion residues in wheat flour samples. Further, to evaluate the efficacy of the proposed method, *in silico* studies were performed to interpret the binding interaction of malathion with insect AChEs.

2. Results and discussion

2.1. Choice of material

For the proposed study a composite of graphitic carbon nitride and nickel chromite was employed to modify the surface of PGE before enzyme immobilization in order to improve the immobilization efficiency, electrical conductivity and catalytic efficiency of bioelectrodes. $NiCr_2O_4$ is a mixed metal oxide that has emerged as a novel material owing to its superior magnetic, electrical, optical and catalytic properties. The transition metal chromite has found potential in a wide range of applications including electrochemical sensors,[33,34] gas sensors,[35] electronic devices,[36] catalytic materials[37] and industrial processes.[38] The incorporation of transition metal oxides on the surface of a potential support material is known to improve their electrocatalytic activity and surface area to volume ratio. The potential of g-C_3N_4 to develop novel nanocomposites with exceptional electrocatalytic and physiochemical properties has been reported by various researchers.[39] The integration of $NiCr_2O_4$ to g-C_3N_4 would cause a unique surface contact between g-C_3N_4 and chromite, resulting in a large electrochemical surface area and accessibility of active sites that would lead to increased electrocatalytic efficiency of the modified electrodes.[40] In addition, considering the role of nickel in specific enzyme immobilization,[41] the composite was expected to possess effective biocatalyst immobilization ability. The $NiCr_2O_4$/g-C_3N_4 composite modified PGE will provide a suitable structure, reactive functional groups and appropriate binding sites for enzyme immobilization in addition to retaining its original activity and stability. Therefore, it will act as a conductive amplifier for enzymes. The principle lies in the EDC/NHS treatment of the material which activates the carboxyl groups

on the surface of the composite, accelerating the formation of amide linkage between the enzyme and modified electrode. Therefore, the composite has dual importance in terms of increasing electrocatalytic efficiency of the biosensor and oriented, site specific immobilization of the enzyme on the modified electrode surface.

2.2. Characterization of the $NiCr_2O_4$/g-C_3N_4 composite

Fig. 2A shows the FTIR spectra of bulk g-C_3N_4, $NiCr_2O_4$ and $NiCr_2O_4$/g-C_3N_4 composite. As shown in Fig. 2A(a) and (b) the FTIR spectra of g-C_3N_4 and $NiCr_2O_4$ exhibit their characteristic absorption peaks as reported earlier.[42,43] For the bulk g-C_3N_4, the peak at 803 cm^{-1} is attributed to out of plane CN heterocyclic bending modes. Besides, the peak at 812 cm^{-1} is attributed to the breathing mode of triazine units. The set of peaks from 1200 to 1400 cm^{-1} are associated with aromatic C–N stretching.[44] The peaks at 1537 and 1627 are attributed to cyano terminal groups C=N group of the triple bond.[45] The broad peak at the right corner at 3156 cm^{-1} has originated due to amine N–H stretching; this is because some nitrogen groups have partially hydrogenated during the calcination process.[46] The absorption band at 663 cm^{-1} is typical of $NiCr_2O_4$ attributed to Ni–O stretching and bending vibrations. The absorption bands at 899 cm^{-1} arise due to Cr–O vibrational modes. The bands at 1631 and 3391 cm^{-1} are ascribed to stretching and bending vibrations of O–H due to adsorption of water molecules to the $NiCr_2O_4$ product. The FTIR spectra of $NiCr_2O_4$/g-C_3N_4 contain characteristic peaks of both $NiCr_2O_4$ and g-C_3N_4, suggesting that $NiCr_2O_4$ particles were embedded on the surface of g-C_3N_4 (Fig. 2A(c)).

To study the crystal structure of the prepared composite material, X-ray diffraction (XRD) patterns of $NiCr_2O_4$/g-C_3N_4 were obtained and compared with those of their individual components, *i.e.* $NiCr_2O_4$ and g-C_3N_4. Typical XRD patterns of the prepared samples are shown in Fig. 2B(a)–(c). All diffraction peaks in $NiCr_2O_4$ can be indexed to a common orthorhombic phase space group *Cmcm* (no. 63) of $NiCr_2O_4$ with lattice constants $a = 5.48$ Å, $b = 8.23$ Å, $c = 6.14$ Å and $\beta = 90°$ (JCPDS no. 072-1605). The diffraction peaks situated at 34.5°, 37.5°, 43.0°, 60.3°, 64.0°, and 71.1° and are indexed to (112), (130), (040), (151), (043) and (204) planes. These results demonstrate a typical XRD pattern of $NiCr_2O_4$. Moreover, g-C_3N_4 forms in the hexagonal shape and is in good agreement with the characteristic peaks (JCPDS no. 87-1526) of g-C_3N_4.[36] Subsequently, the XRD pattern for $NiCr_2O_4$/g-C_3N_4 compared with $NiCr_2O_4$ and g-C_3N_4 showed two diffraction peaks at 27.6° and 13.0° that are indexed to (002) and (100) planes, confirming the presence of g-C_3N_4 with $NiCr_2O_4$. The two sample peaks have been marked with different symbols (+) and (*) to confirm their presence.

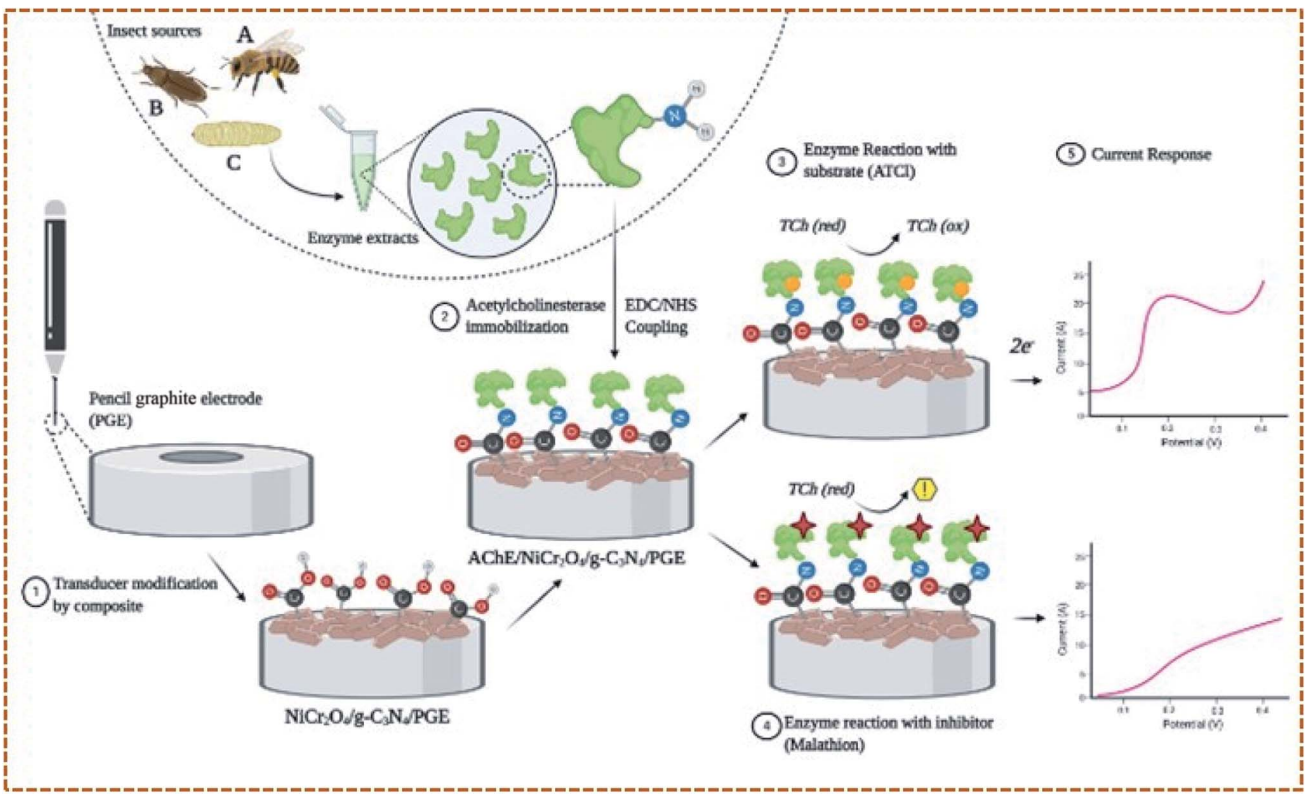

Fig. 1 Principle diagram of the steps involved in the preparation of an electrochemical biosensor utilizing acetylcholinesterase (AChE) from three different enzyme sources *i.e.* (A) *Apis mellifera* (referred to as Am-AChE), (B) *Tribolium castaneum* (referred to as Tc-AChE) and (C) *Zootermopsis nevadensis* (referred to as Zn-AChE) immobilized on the surface of the $NiCr_2O_4$/g-C_3N_4 composite modified pencil graphite electrode (PGE). The illustration was created using https://Biorender.com.

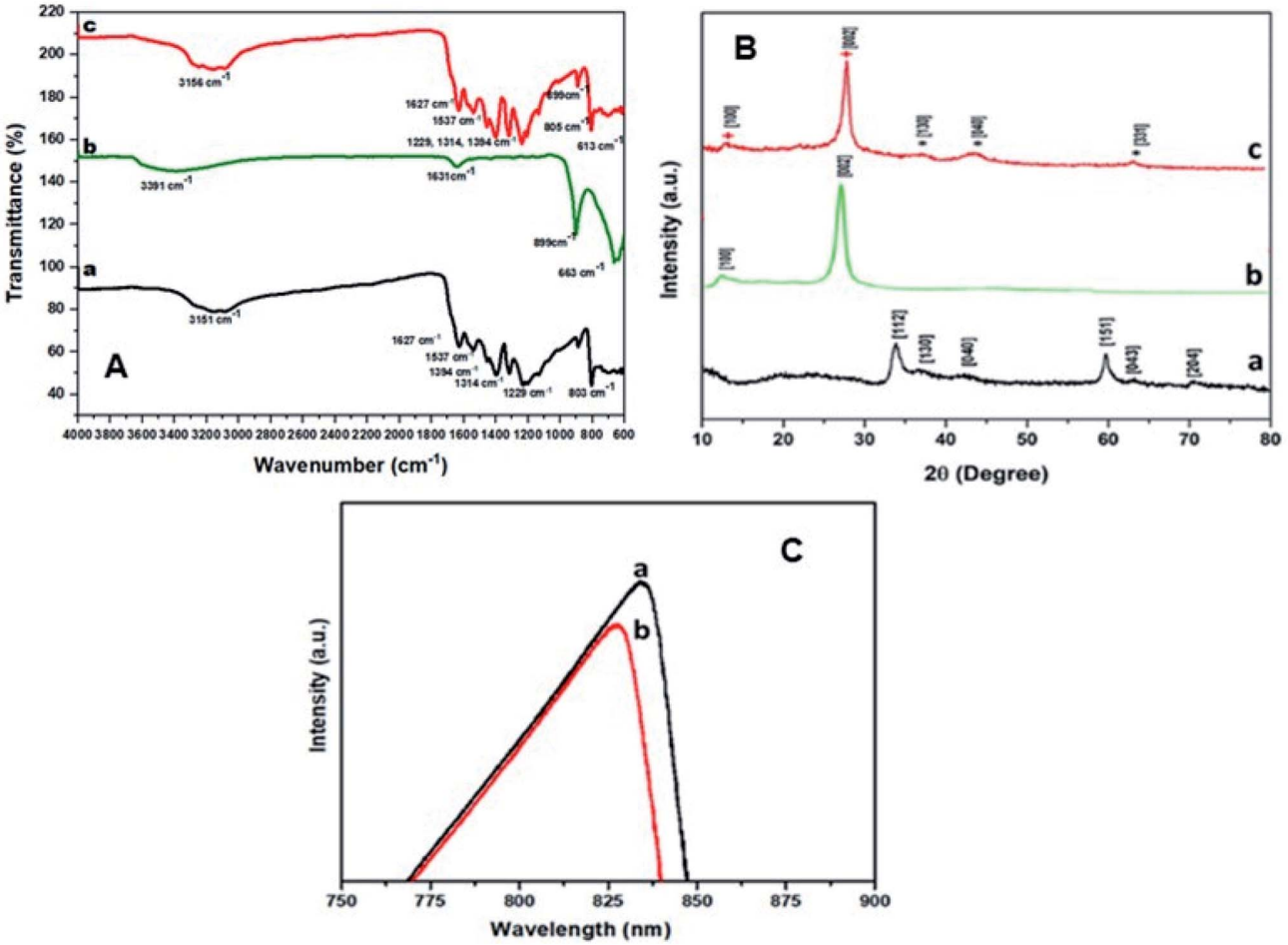

Fig. 2 (A) FTIR spectra of (a) g-C_3N_4, (b) $NiCr_2O_4$, and (c) $NiCr_2O_4$/g-C_3N_4 composite. (B) XRD patterns of (a) g-C_3N_4, (b) $NiCr_2O_4$, and (c) $NiCr_2O_4$/g-C_3N_4 composite. (C) PL spectra of (a) g-C_3N_4 and (b) $NiCr_2O_4$/g-C_3N_4 composite.

Fig. 2B demonstrated less intense peaks of $NiCr_2O_4$ because the g-C_3N_4 peak is much higher and sharper, and it is a common observation that the peak intensities become weaker at larger angles and besides that micro strain broadening is also large at larger angles; therefore, some peaks of $NiCr_2O_4$ become broader at higher angles and are less noticeable in the pattern.

The PL spectra of g-C_3N_4 and $NiCr_2O_4$/g-C_3N_4 composite are shown in Fig. 2C. It can be seen that g-C_3N_4 had a broad and strong peak at around 833 nm, while $NiCr_2O_4$ at around 827 nm. It can be clearly observed that g-C_3N_4 produced higher intensity spectra than the $NiCr_2O_4$/g-C_3N_4 composite, which clearly indicates the increased efficiency of separation of charge carriers. This relates to the participation of more electrons and holes in oxidation and reduction reactions.[47] The higher intense peak exhibits faster recombination of electrons and holes, thus lower redox reactions, while compared to the above a weaker and lower $NiCr_2O_4$/g-C_3N_4 composite depicts slow recombination of electrons and holes, indicating higher redox reactions.[48]

Further, the morphological nature and microstructure of the as-prepared $NiCr_2O_4$/g-C_3N_4 composite were inspected by SEM analysis and compared with those of its individual components, as shown in Fig. 3. Furthermore, the elemental composition of the as-prepared materials was also investigated by EDS analysis. It can be seen in Fig. 3A and B that the bulk g-C_3N_4 is in the form of irregular, rough, aggregated sub-blocks and stacked layers. Fig. 3A shows a rough and fissured morphology with lots of agglomerated particles of around 1.7 μm size. Some flaked stacks can also be seen which may have formed during the heating process of melamine, where HCL and NH_3 were released which may hinder the thermal condensation into g-C_3N_4 sheets.[49,50] Interestingly, some tubular stacked flake shaped structures also appeared on the surface with holes alongside, which can be seen in Fig. 3B. As discussed earlier the holes may be formed due to the release of ammonia and HCL gasses during the heating of melamine.[50] The average size of these tubular stacked flakes is 0.81 μm. Fig. 3D shows the SEM image of $NiCr_2O_4$ and it can be clearly seen that spherical pumice stone shaped particles formed with diameters up to 0.96 μm. The particle agglomeration also happened which may be due to incomplete synthesis. The spongy surface of the particles, which can be seen in Fig. 3E, is linked to high reactivity of the catalyst due to the presence of numerous reaction sites. The SEM images of the $NiCr_2O_4$/g-C_3N_4 composite are shown in Fig. 3G and H. It can be seen that $NiCr_2O_4$ particles are evenly

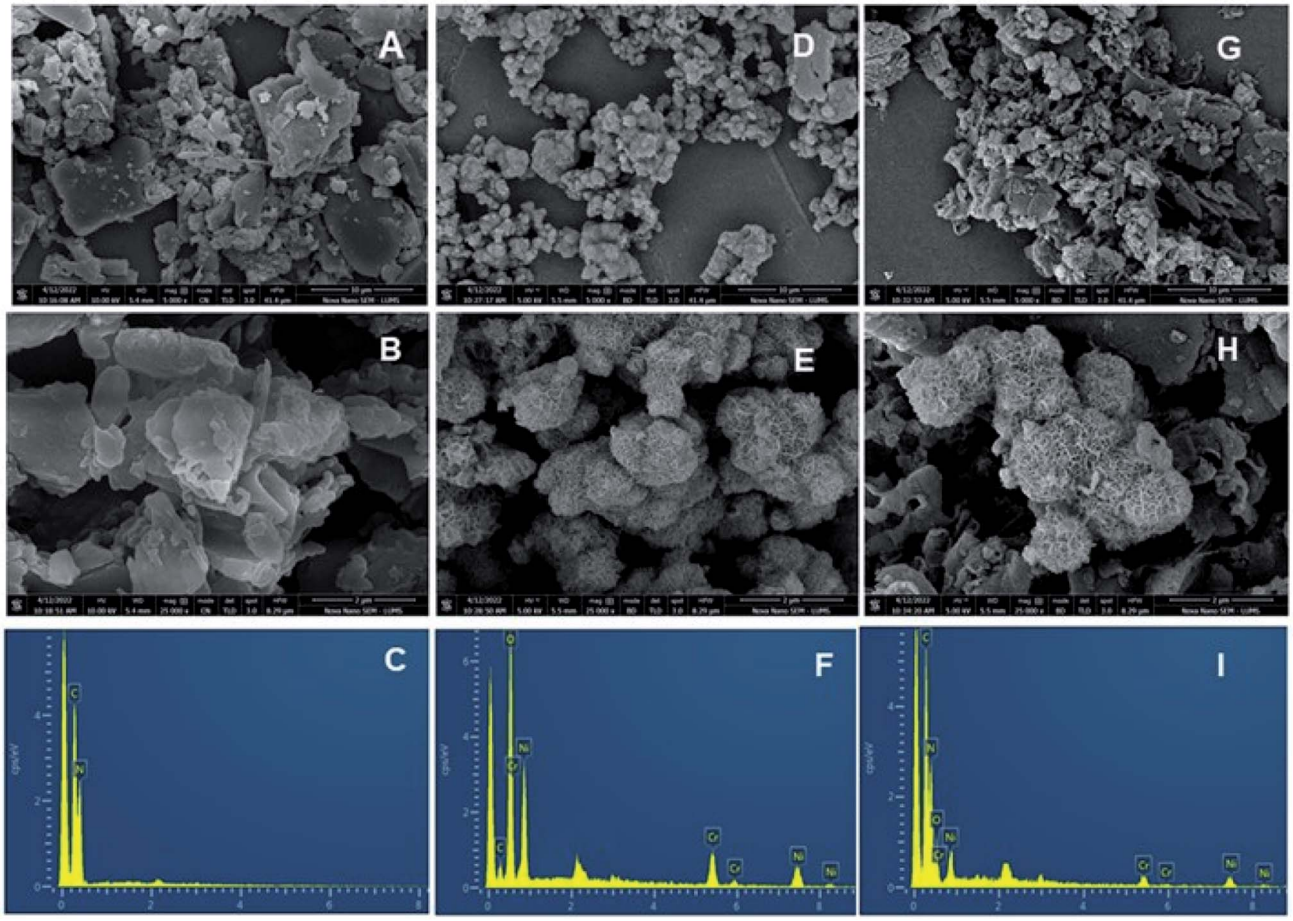

Fig. 3 SEM micrographs of (A) g-C_3N_4 at 10 μm resolution, (B) g-C_3N_4 at 2 μm resolution, (C) energy dispersive spectrum of g-C_3N_4 showing the presence of C and N in the spectrum, (D) SEM images of $NiCr_2O_4$ at 10 μm resolution, (E) $NiCr_2O_4$ at 2 μm resolution, (F) energy dispersive spectrum of $NiCr_2O_4$ showing the presence of Ni, O, and Cr in the spectrum, (G) SEM images of the $NiCr_2O_4$/g-C_3N_4 composite at 10 μm resolution, (H) $NiCr_2O_4$/g-C_3N_4 composite at 2 μm resolution, and (I) energy dispersive spectrum of the $NiCr_2O_4$/g-C_3N_4 composite showing the presence of C, N, Ni, O, and Cr in the spectrum confirming successful synthesis of the composite.

distributed on the surface of g-C_3N_4 flakes. In Fig. 3G the bright particles also confirmed the presence of $NiCr_2O_4$ which was previously undermined in the XRD spectra of the composite. This indicates that g-C_3N_4 acts like a sheet to support $NiCr_2O_4$ particles, which are attached and formed interconnects to behave like a single catalyst.[47] Thus it can be conferred that the $NiCr_2O_4$/g-C_3N_4 composite with excellent nanojunctions has been successfully synthesized that would result in high electrocatalytic activity of the $NiCr_2O_4$/g-C_3N_4 composite due to efficient transfer of electrons during the electrochemical reaction.[36,51,52] Further, energy-dispersive spectra of the composite and its components (Fig. 3C, F and I) revealed the presence of respective elements in the respective materials and confirmed the purity and successful synthesis of the as-prepared composite.

2.3. Electrochemical characterization of electrodes

Electrochemical characterization of bioelectrodes at each fabrication step was done by cyclic voltammetry using a 5 mM equimolar solution of $Fe(CN)_6^{3-/4-}$ while potential swept across −0.8 to +0.8 V. The resistance to electron flow was measured by EIS at amplitude 234. It can be seen in Fig. 4A by the CV response that the current passing through bare PGE, GCN/PGE and Ni/GCN/PGE was subsequently increased, and the conductivity of the Ni/GCN modified pencil electrode was highest; similarly, the Nyquist plots (Fig. 4B) showed that resistance decreased in the same manner as the current was increased, whereas when the composite was functionalized with carboxyl groups, the resistance to electron flow enhanced, resulting in reduced current which ascertains successful introduction of carboxyl functional groups on the composite surface.

After coating AChE on Ni/GCN/PGE, the value of peak current of AChE/Ni/GCN/PGE was decreased as shown in Fig. 4C, which verifies the attachment of the enzyme on the electrode surface. The attachment causes an increase in interface thickness, causing an interruption in electron flow and thus high impedance as shown by the EIS spectra of bioelectrodes in Fig. 4D. The results confirm the inertness of the enzyme molecule as it is not itself oxidized or reduced during the voltage cycling. As the source of AChE was three different

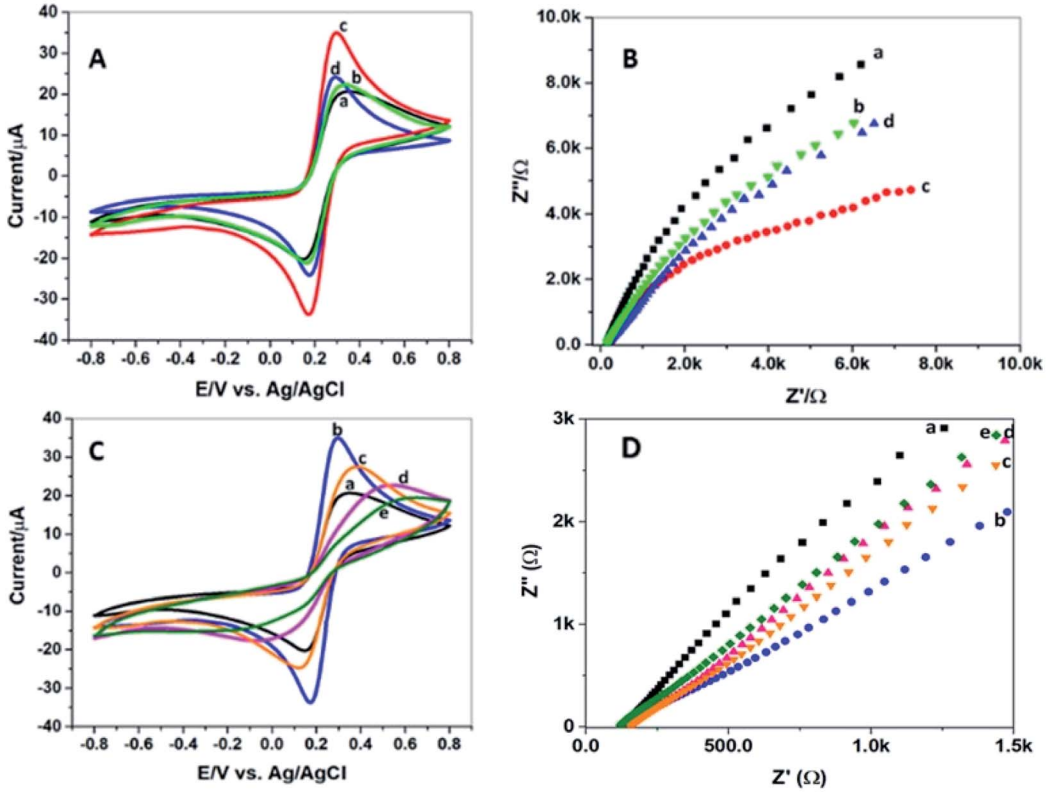

Fig. 4 (A) Cyclic voltammograms and (B) EIS Nyquist plots of bare PGE (a), GCN (b), Ni/GCN (c) and functionalized Ni/GCN-COOH (d) in 5 mM $[Fe(CN)_6]^{3-/4-}$ solution comprising 0.1 M KCl and pH 7.4 PBS, (C) cyclic voltammograms and (D) EIS Nyquist plots of bare PGE (a), functionalized Ni/GCN-COOH (b), Am-AChE/Ni/GCN/PGE bioelectrode (c), Tc-AChE/Ni/GCN/PGE bioelectrode (d), and Zn-AChE/Ni/GCN/PGE bioelectrode (e) in 5 mM $[Fe(CN)_6]^{3-/4-}$ solution comprising 0.1 M KCl and 0.1 M pH 7.4 PBS.

insects, the electrochemical response of all three fabricated interfaces, *i.e.* Am-AChE/Ni/GCN/PGE, Tc-AChE/Ni/GCN/PGE, and Zn-AChE/Ni/GCN/PGE was determined, and the peak oxidation current of thiocholine was found to be different among them. It was noticed that current was decreased maximally in the case of *Z. nevadensis* AChE (Zn-AChE) compared to *T. castaneum* AChE (Tc-AChE), and least in the case of *A. mellifera* AChE (Am-AChE). The impedance increased in the same reverse order (Fig. 4D). The results confirmed good electrical conductivity of the composite and successful immobilization of each component of the biosensor.

2.4. Analytical behavior of integrated bioelectrodes

It is important to measure the electro-catalytic behaviour of the prepared bioelectrodes in response to thiocholine, which is the electroactive hydrolysis product of the AChE reaction and is responsible for electrochemical activity. For this purpose, CV was run for the AChE/Ni/GCN/PGE biosensor in the presence and absence of the substrate, ATCl. The response of three types of bioelectrodes, *i.e.* Am-AChE/Ni/GCN/PGE, Tc-AChE/Ni/GCN/PGE and Zn-AChE/Ni/GCN/PGE, was compared in the presence of ATCl. As shown in Fig. 5, the current response of the bare electrode and negative controls did not produce any obvious oxidation peaks; however, in the case of Zn-AChE/Ni/GCN/PGE, a reversible oxidation peak arises at 0.7 V, whereas in Tc-AChE/Ni/GCN/PGE, a peak at 0.74 V can be observed. An obvious oxidation peak at 0.79 V was observed in Am-AChE/Ni/GCN/PGE with the highest peak signal compared to Tc-AChE and Zn-AChE.

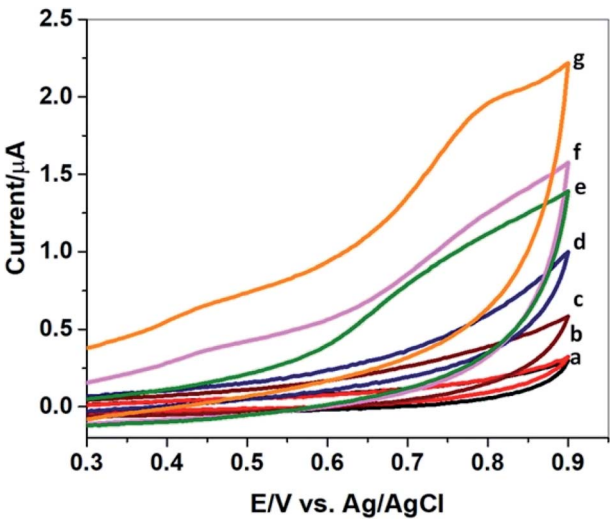

Fig. 5 Cyclic voltammograms of bare PGE in pH 7.4 PBS (a), bare PGE in pH 7.4 PBS containing ATCl (b), Ni/GCN/PGE in pH 7.4 PBS (c), Ni/GCN/PGE in pH 7.4 PBS with ATCl (d), Zn-AChE/Ni/GCN/PGE (e), Tc-AChE/Ni/GCN/PGE (f), and Am-AChE/Ni/GCN/PGE (g) in pH 7.4 PBS containing ATCl.

The absence of the oxidation peak in negative controls confirmed that the anodic peak was coming from the hydrolysis product of AChE, *i.e.* TCh. It can be inferred that AChE activity is considerably high in *A. mellifera*, and it provides suitable attachment sites, structural and surface features that stabilize protein conformation and orientation, providing efficient immobilization on the surface of the Ni/GCN modified electrode.

2.5. Experimental optimization

The optimum experimental parameters were set in order to ensure the best performance of fabricated biosensors. In order to improve the analytical efficiency of the biosensor, the incubation time of the material was validated by incubating the bioelectrodes in composite suspension for a time period of 60 minutes. Fig. 6A shows that 15 minutes is a suitable time to achieve a better current response.

Moreover, from Fig. 6B we could find that by increasing scan rate from 10 to 125 mV s^{-1}, the peak current increased subsequently and the plots of square root of scan rate and current showed a linear response with the regression equation $y = 0.2612x + 0.2381$ ($R^2 = 0.9865$), which indicates a surface controlled electrochemical process on the electrode, which means that the composite provides a conductive pathway and a large surface area for the effective immobilization of the enzyme on the electrode surface. However, 50 mV s^{-1} was used for all electrochemical measurements.

Similarly, the optimum incubation time of enzyme deposition was also determined to be 15 minutes (Fig. 6C). It was observed that under the given conditions, the current for the oxidation of acetylcholine increased with the increase in immobilization time of the enzyme; however, after 15 minutes a decrease in oxidation peak current was noticed probably due to interruption in current flow after a saturation point for the enzyme was achieved.

Further, the appropriate amount of extract that can be used for AChE was determined, because the amount of enzyme plays an important role in biosensor fabrication due to its insulating nature and possibility of increased film thickness. The varying amount of extracts of *A. mellifera*, *T. castaneum* and *Z. nevadensis* was deposited on the electrode surface, and 0.8 mg μL^{-1} was found suitable to obtain sufficient oxidation peak current (Fig. 6D).

The pH of phosphate buffer was adjusted at 7.4 for all electrochemical measurements. To ensure the maximum degree of

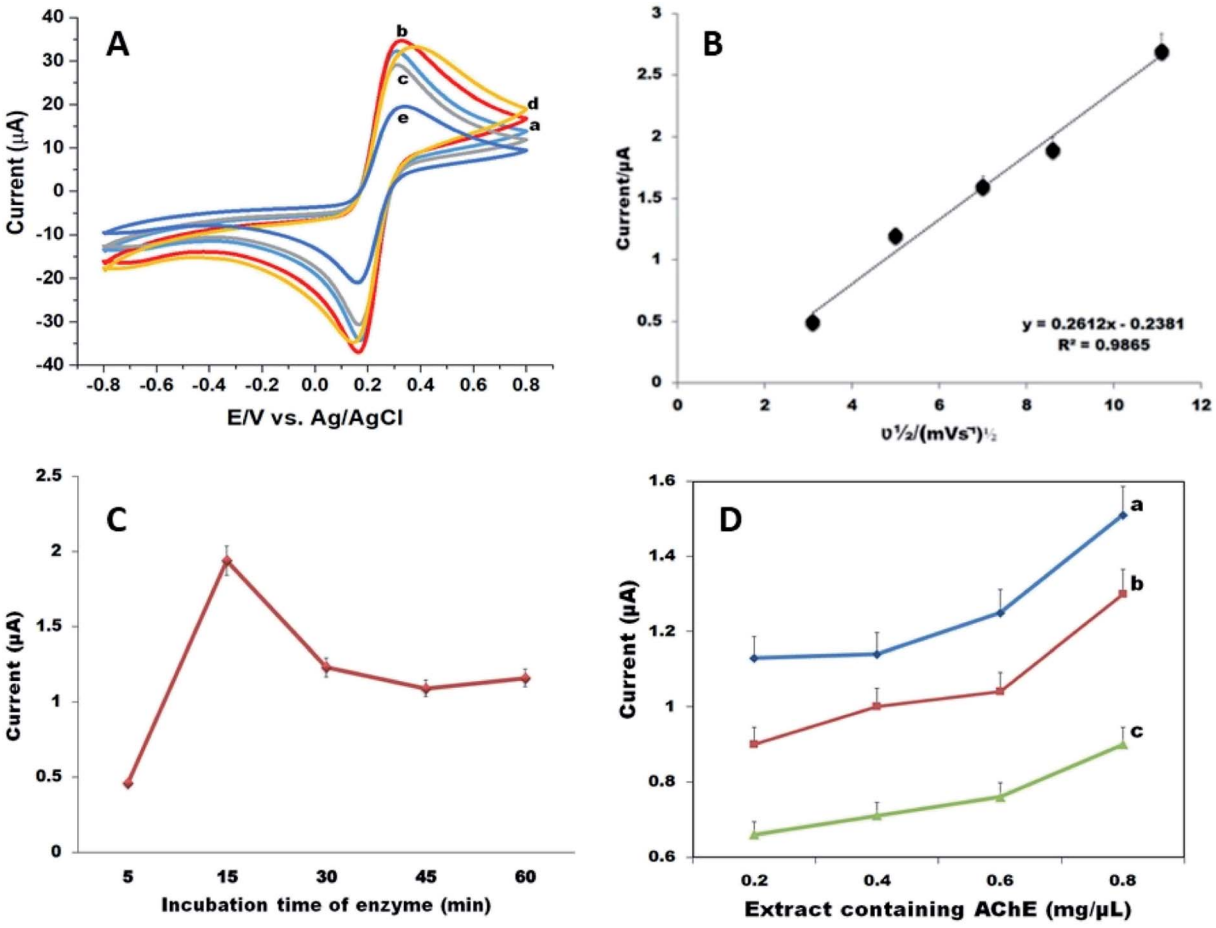

Fig. 6 (A) Effect of incubation time on the CV response of fabricated bioelectrodes, (B) plot of current *vs.* square root of scan rate, (C) effect of incubation time on the performance of AChE activity, and (D) amount of extracts *A. mellifera* (a), *T. castaneum* (b) and *Z. nevadensis* (c) as the AChE source immobilized on the pencil electrode surface.

enzyme inhibition, the effect of inhibition time was determined and it was observed that after 15 minutes of biosensor incubation with malathion, the degree of inhibition increased, after which it was stabilized by virtue of saturated binding between the active sites of the enzyme and pesticides (Fig. 8A). Thus, 15 min was employed for malathion inhibition assay.

2.6. Calibration curve of ATCl and enzyme kinetics

The influence of substrate concentration on the analytical performance of biosensors is an important parameter to determine the performance and sensitivity of the biosensor. A plot of current *versus* ATCl concentration is useful to determine the kinetics of the enzymatic reactions. The current response produced by the product of enzymatic catalysis corresponds to the velocity of the enzymatic reaction, which is proportional to the activity of the immobilized enzyme, according to the Michaelis–Menten equation. The effect of ATCl concentration was investigated with the already standardized parameters by varying its amount from 0.5 mM to 8 mM in 0.1 M pH 7.4 PBS. The substrate concentration at which the maximum current response obtained was different for each insect; therefore, detection limits and sensitivities for each biosensor were also different (Fig. 7A). For Am-AChE/Ni/GCN/PGE, the maximum current response was obtained at 2 mM, whereas in the cases of Zn-AChE/Ni/GCN/PGE and Tc-AChE/Ni/GCN/PGE, the maximum current response was attained at 6 mM and 8 mM, respectively. All readings were taken in triplicate with RSD < 4% ($n = 3$). The sensitivities of Am-AChE/Ni/GCN/PGE, Tc-AChE/Ni/GCN/PGE and Zn-AChE/Ni/GCN/PGE were calculated to be 62.27, 22.29 and 22.41 μA mM^{-1} cm^{-2}, respectively. To determine the affinity of the enzyme for the substrate, the apparent Michaelis–Menten constant (Km^{app}) was calculated for each biosensor from the slope and intercept for the reciprocal plots of the steady-state current *vs.* ATCl concentration (Fig. 7B). The Km^{app} for Am-AChE/Ni/GCN/PGE, Zn-AChE/Ni/GCN/PGE and Tc-AChE/Ni/GCN/PGE was 140 μM, 0.41 mM and 0.46 mM, respectively. It can be inferred from the results that honeybee AChE has higher affinity and sensitivity for the ATCl than red flour beetle and termite AChE, which have almost equal affinity for the substrate. However, the values are quite low and comparable to those of many other reported biosensors as shown in Table 1, which ensures good analytical behaviour and sensitivity of proposed biosensor platforms on account of the exceptional catalytic efficiency of the Ni/GCN composite using insect enzyme sources.

2.7. Electrochemical test for malathion sensitivity

To investigate the applicability of proposed biosensors for organophosphorus pesticide detection, the modified bioelectrodes were incubated with different concentrations of malathion under optimized conditions and CV responses were recorded (Fig. 8). The linear ranges for three types of biosensors were different. The linear range for Am-AChE/Ni/GCN/PGE, Tc-AChE/Ni/GCN/PGE, and Zn-AChE/Ni/GCN/PGE was 0.1–1.6 μM,

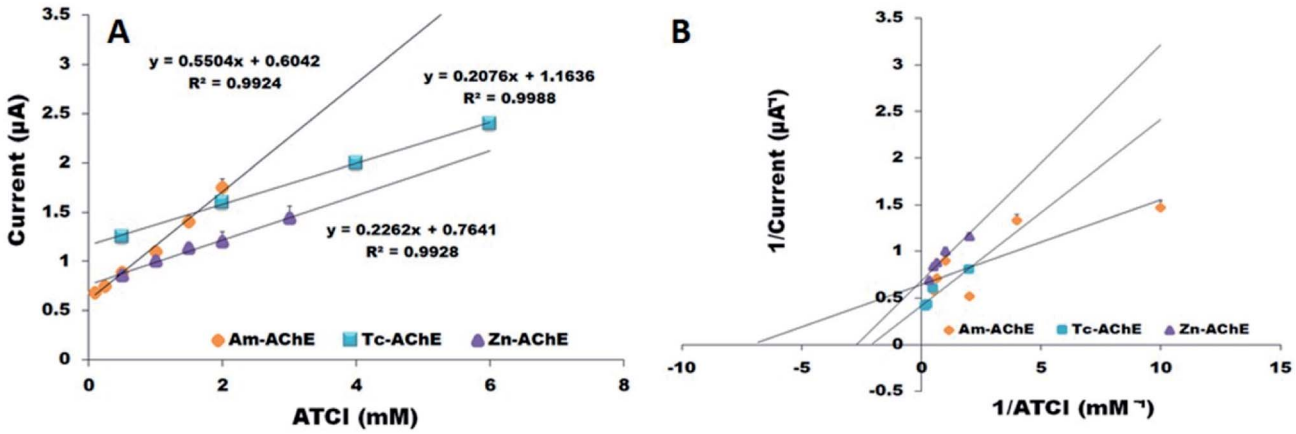

Fig. 7 (A) Calibration curves of ATCl in pH 7.4 PBS for Am-AChE/Ni/GCN/PGE (a), Tc-AChE/Ni/GCN/PGE (b), and Zn-AChE/Ni/GCN/PGE (c); (B) the Lineweaver–Burk plot of 1/current *vs.* 1/ATCl for Am-AChE/Ni/GCN/PGE (a), Tc-AChE/Ni/GCN/PGE (b), and Zn-AChE/Ni/GCN/PGE (c).

Table 1 Km^{app} and sensitivity of reported AChE modified electrodes and our proposed AChE/Ni/GCN modified PG electrodes

Biosensor platform	Km^{app}	Sensitivity	Reference
AChE/$Ti_3C_2T_x$-CS/GR/GCE	4.89 mM	NR	53
AChE/3D tree-like Ag/GCE	137.5 μM	0.056 μA mM^{-1}	54
AChE-Chit/Pd@Au NWsN/GCE	190 μM	NR	55
f-MWCNT/poly(SNS-NH_2)/AChE	1.038 mM	24.16 μA mM^{-1} cm^{-2}	56
Am-AChE/Ni/GCN/PGE	140 μM	62.27 μA μM^{-1} cm^{-2}	This work
Tc-AChE/Ni/GCN/PGE	0.46 mM	22.29 μA mM^{-1} cm^{-2}	This work
Zn-AChE/Ni/GCN/PGE	0.41 mM	22.41 μA mM^{-1} cm^{-2}	This work

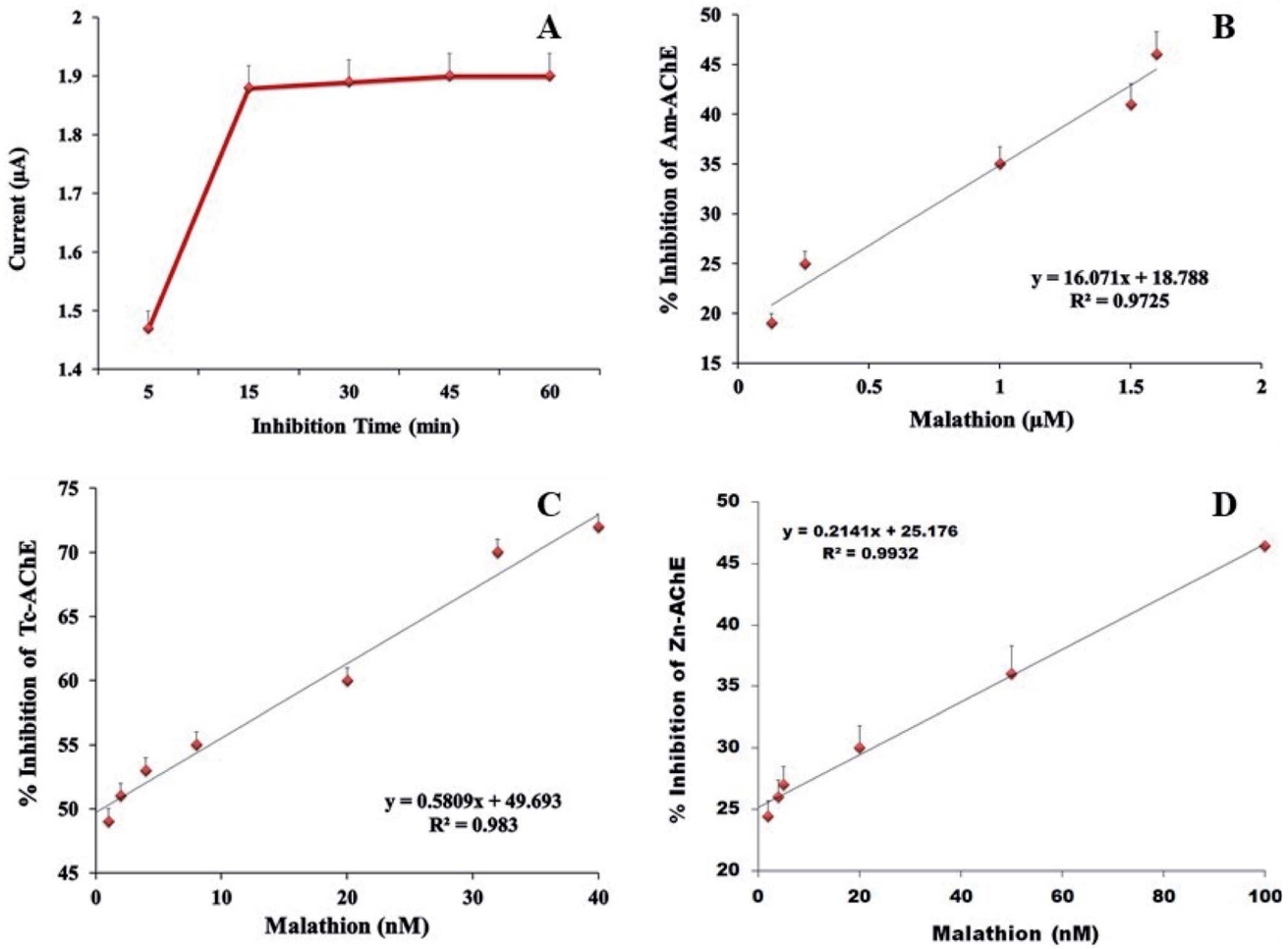

Fig. 8 (A) Incubation time optimization for malathion, and (B) the calibration curve for malathion detection by (C) Am-AChE/Ni/GCN/PGE, (D) Tc-AChE/Ni/GCN/PGE, and (E) Zn-AChE/Ni/GCN/PGE.

1–40 nM, and 2–100 nM respectively. The LOD and LOQ values for each biosensor were determined by the method based on the standard deviation of the current response and the slope of the calibration line. The LODs were found to be 2 nM, 0.86 nM and 2.3 nM and LOQs were 6 nM, 2.6 nM, and 7 nM for Am-AChE/Ni/GCN/PGE, Tc-AChE/Ni/GCN/PGE, and Zn-AChE/Ni/GCN/PGE, respectively. Similarly, the detection sensitivities were 1607, 58.09 and 21.4 μA nM^{-1} cm^{-2} for Am-AChE/Ni/GCN/PGE, Tc-AChE/Ni/GCN/PGE, and Zn-AChE/Ni/GCN/PGE, respectively. A high detection limit for Am-AChE/Ni/GCN/PGE may result from many factors such as population genetics or insecticide resistance among these insects. Previous reports have shown unique behaviours of honeybee enzymes towards certain insecticides and it has been found that many organic and chemical pesticides pose limited toxicity to honeybees, while others are highly toxic towards them, whereas the *T. castaneum* AChE is more susceptible to organophosphates and the genes and structure of AChE are widely studied in these insects.[57–60] The insects damage a large mass of stored grains each year and multiply in large amounts in a very short time. In addition, they develop insecticide resistance, resulting in reduced sensitivity against insecticides. Based on its potential, the insect has been used in our previous study for the construction of biosensors for OP detection.[21] Further, the damp wood termite species used in this study have not been significantly studied for their enzymes and the impact of pesticides on them. Even though the results indicate a similar inhibition pattern to *T. castaneum* AChE, the linear range for detection is wider than that for Tc-AChE. It can be recommended from the results that the platform is highly suitable to study the behaviour of insects' AChE towards OPs and can be utilized for all forms of AChEs. The result for Am-AChE suggests that the sensing design exhibits properties useful for organophosphate determination for commercial applications in honeybee populations contaminated by pesticides. The analytical performance of the proposed platforms was even better than that of various previously reported biosensor platforms for malathion detection (Table 2). Moreover, the presented design is tested on stored grains such as wheat for its practicality, which has not been done before.

2.8. Real time detection of malathion from wheat flour

The potential application of the proposed biosensor was demonstrated by detecting malathion in real samples of whole-wheat flour, which was not contaminated with pesticides. A

Table 2 A comparison of linear range and LOD of proposed biosensor platforms with other reported biosensors for malathion detection

Malathion biosensor	Linear range	LOD	References
AChE-PANI/ZnO/RGO/GCE	10–40 nmol L^{-1}	11 nmol L^{-1}	61
CHIT-g-PANI based electrode	2–62.5 μM	3.8 μM	62
AChE/HCS@PANI/GCEAChE/HCS@PANI/GCE	1.0–10 μg mL^{-1}	0.16 ng mL^{-1}	47
poly(TTP)/AChE/GCE	9.99–99.01 nM	4.08 nM	63
PANI-ES SWCNTS/GE	0.2–1.4 μM	0.2 μM	64
Am-AChE/Ni/GCN/PGE	0.1–1.6 μM	2 nM	This work
Tc-AChE/Ni/GCN/PGE	1–40 nM	0.86 nM	This work
Zn-AChE/Ni/GCN/PGE	2–100 nM	2.3 nM	This work

Table 3 Determination of malathion in spiked wheat flour samples through the biosensor method and comparison of recovery values with the standard HPLC method

Source	Added (μM)	Found (μM)	% Recovery	RSD%
Biosensor method				
Apis mellifera (honeybee)	(i) 0.128	0.127	99.2	3.2
	(ii) 1	1.009	100.9	2.1
	(iii) 1.6	1.594	99.6	4.1
HPLC method				
Apis mellifera (honeybee)	(i) 0.128	0.128	100	3.9
	(ii) 1	0.99	99	3.0
	(iii) 1.6	1.61	100.6	3.6

standard addition method was employed to detect wheat samples for different concentrations of malathion. The Am-AChE/Ni/GCN/PGE biosensor exhibited good practical application showing good reliability with the recovery ranging from 99 to 100.9%, as well as RSDs less than 5% (Table 3). The other two interfaces did not provide satisfactory recoveries of malathion from wheat samples and therefore are not included here. The liability of the proposed method was assessed by comparing the obtained results with HPLC as a reference method, and the results were comparable as shown in Table 3. The results showed that the Am-AChE/Ni/GCN/PGE biosensor is most effective in recovery for malathion in real agricultural samples.

2.9. Selectivity and reproducibility

The selectivity of the biosensor was assessed by recording the current responses of Am-AChE/Ni/GCN/PGE in the presence of possible interfering analytes in the environment, like urea, uric acid, metal ions and transition metal ions. It can be seen in Fig. 9A that the interfering substances did not display any considerable disturbance in the current signals in the presence of 2 mM ATCl. Moreover, the current response of malathion in the presence of interfering substances was also investigated which did not get affected significantly; therefore, the results were not added in the manuscript. The obtained results propose an outstanding anti-interference capability of the biosensing interface.

The precision was evaluated by evaluating the current response of five different electrodes using the same concentration of malathion and the RSD was acquired <5% ($n = 4$), showing good operational reproducibility of the biosensor (Fig. 9B). The above results validated a good reproducibility of the devised method.

2.10. Docking studies for AChE–malathion interaction

The study of the physicochemical properties of an enzyme and its structural and surface features is also very important to

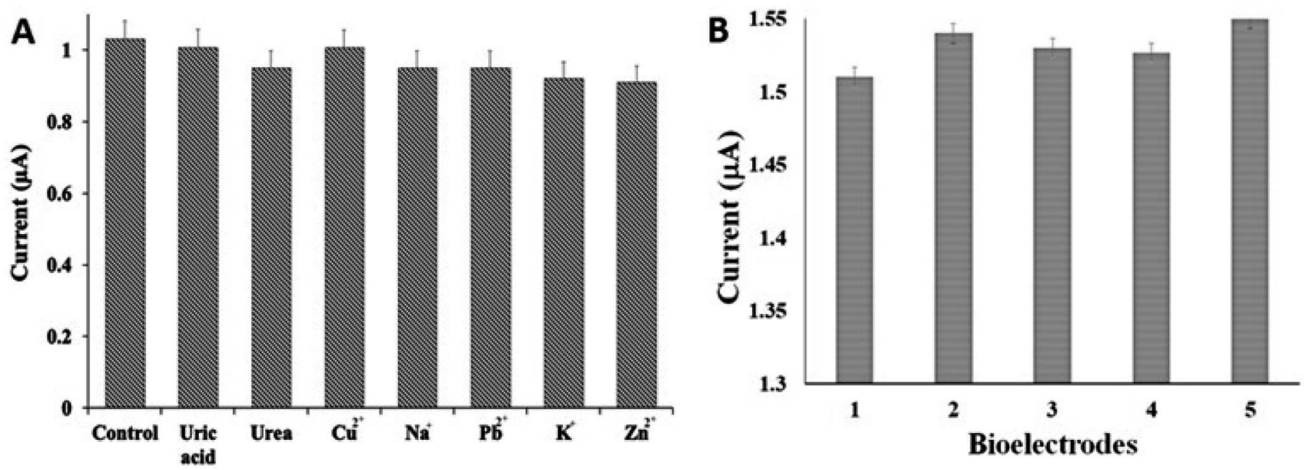

Fig. 9 (A) CV current responses in pH 7.4 PBS containing 2 mM ATCl without and with the interfering substances. (B) CV current responses of five bioelectrodes in pH 7.4 PBS containing 2 mM ATCl to test the reproducibility of the results.

predict the immobilization efficiency of an enzyme on the transducer surface. AChE is a comparatively hard protein with a high degree of hydrophobicity that helps its binding on the hydrophobic substrates, prevents denaturation, and improves its thermal stability. Such immobilizations are known to improve organophosphate detection more efficiently. Furthermore, amino acids can form coordination metal complexes through their amino and carboxylate functional groups, while side chains of some amino acids possess metal-binding groups such as the imidazole ring of His or phenol ring of Tyr. For this study, the AChE has been immobilized through EDC/NHS chemistry, causing covalent binding of amine groups of AChE amino acids to the carboxylate-modified composite material. Moreover, the complexation of Ni with amino acids possibly improves the immobilization and catalytic efficiency of enzymes with the transducer surface. The imidazole ring of His and thiol sulfur group of Cys coordinates with Ni and is crucial for the interactions between peptides and Ni through amino or amide nitrogen atoms.[65–67] Therefore, the offered transducer surface not only helps in catalysis and improved conductivity but also provides a suitable binding site for efficient enzyme immobilization with disturbing the structure of active sites, making them available to bind with the analyte molecules.

Further, to gain an insight into the binding interaction of the model pesticide, malathion, with the amino acid residues of AChE enzymes of source insects, molecular docking simulations were performed. The molecular docking analyses show that malathion interacts with all three acetylcholinesterase enzymes, *i.e.*, Tc-AChE, Am-AChE1, and Zn-TChE. The binding energies of malathion for Tc-AChE, Am-AChE1, and Zn-TChE were found to be −5.73, −5.95, and −5.54 kcal mol^{-1}, while the dissociation constants were 62.6, 43.5, and 87.1 μM, respectively.

Malathion interactions with Am-AChE1 show that ASN^{117} and TYR^{385} are involved in the formation of two H-bonds (3.47 and 3.17 Å) with oxygen atoms of malathion, while other surrounding residues, including GLY^{168}, GLY^{167}, GLY^{112}, GLU^{113}, TRP^{116}, PHE^{386}, TYR^{389}, TYR^{179}, GLU^{252}, and TYR^{104}, are involved in stabilizing the interactions (Fig. 10A). TYR^{185} and TRP^{344} are present at the entrance gorge. The same amino acids have been previously reported to form the Am-AChE1 active site.[68]

In the case of Tc-AChE, O4 in malathion forms a comparatively strong H-bond (2.95 Å) with the backbone amine of TYR^{189}, present at the opening of the active site gorge of Tc-AChE, therefore blocking the ATC entry site. Moreover, GLY^{187}, GLY^{186}, ASN^{153}, ALA^{149}, ASP^{140}, ILE^{139}, ALA^{508}, TRP^{152}, GLU^{266}, SER^{267}, TYR^{396}, PHE^{397}, and HIS^{507} were involved in the stabilization of the ligand–enzyme complex (Fig. 10B). Previously, Phosmet was also found to make H-bonding with Tyr^{189} and Ser^{190} of Tc-AChE.[21] Distal methyl groups in malathion were found to bind deep in the active site gorge and show hydrophobic interactions with GLY^{187}, SER^{256} and TRP^{300}. Previously, azadirachtin, a saponin from *Azadirachta indica*, was found to interact with Tc-AChE with lower binding affinities and at different binding sites.[4,69] In our study, malathion was also found to bind acetylthiocholine active site residues mentioned

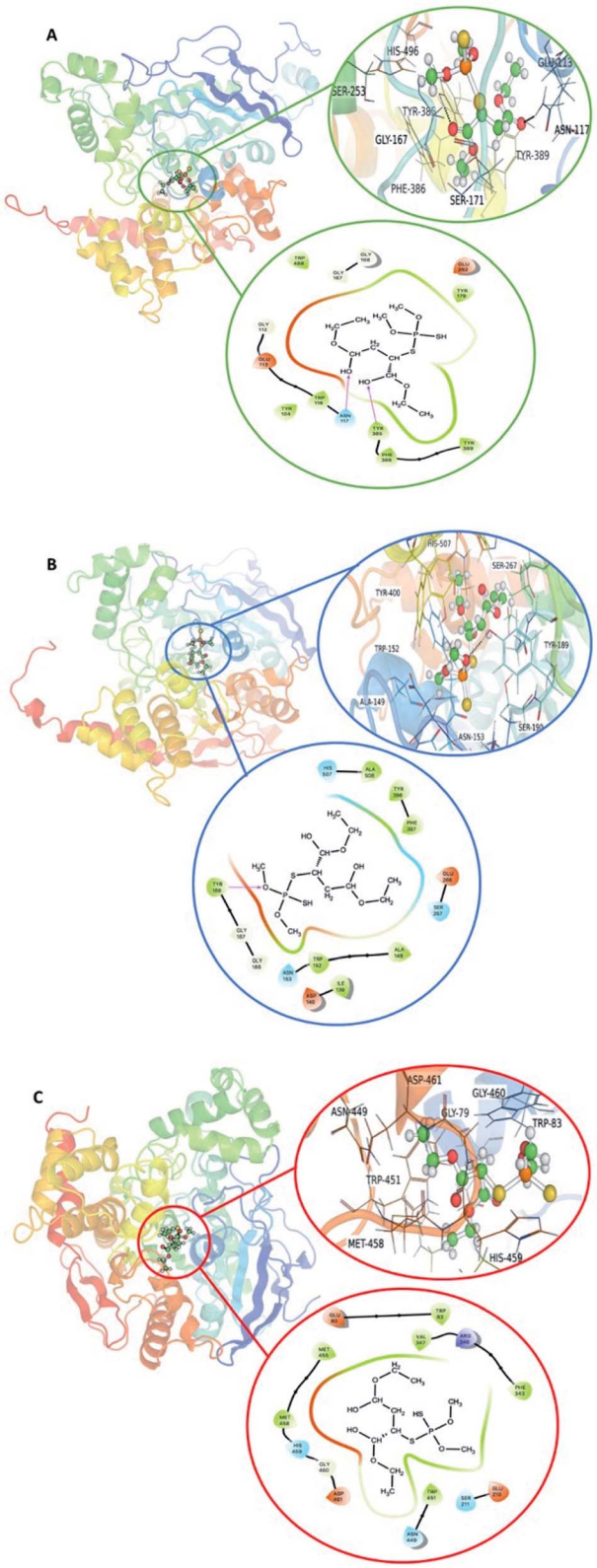

Fig. 10 Molecular docking analysis of (A) Am-AChE1, (B) Tc-AChE, and (C) Zn-AChE with malathion. The upper insets show a close-up view of amino acid residues interacting with malathion, while the lower inset presents the protein-ligand interaction diagram showing binding mode affinities of the ligand with the receptor where H-bond (backbone) is indicated with purple arrows.

by ref. 21, with comparatively less affinity (−5.54 kcal mol^{-1} binding energy and 84.8 μM dissociation constant), including ILE^{138}, ASP^{140}, ILE^{139}, ALA^{149}, TRP^{152}, ASN^{153}, GLY^{185}, GLY^{186}, GLY^{187}, TYR^{189}, SER^{190}, GLU^{266}, SER^{267}, ALA^{268}, TYR^{396}, PHE^{397}, TYR^{400}, TRP^{449}, HIS^{507}, and ALA^{508}. Surprisingly, when 300 ppm (~1 mM) malathion was used against *T. castaneum*, an 11-fold increase in Tc-AchE activity was found.[70] Our molecular docking results may explain the reason for this increased Tc-AChE activity; the dissociation constant of malathion–Tc-AChE was found to be 62.6 μM, while at high concentrations, malathion binds nonspecifically at various sites in Tc-AChE that may bring conformational changes in enzyme structure and augment its activity. Malathion also interacts with Zn-AChE, while binding on the surface interactions is stabilized by GLU^{80}, TRP^{83}, GLU^{295}, SER^{211}, PHE^{343}, ARG^{346}, VAL^{347}, ASN^{449}, MET^{458}, HIS^{459}, GLY^{460}, and ASP^{461} residues (Fig. 10C).

3. Materials and methods

3.1. Chemicals

Analytical grade acetylthiocholine chloride (ATCl), potassium ferricyanide ($K_3[Fe(CN)_6]$), potassium ferrocyanide ($K_4[Fe(CN)_6]$), malathion, $Na_2Cr_2O_7$ and Ni_2SO_4 were purchased from Sigma-Aldrich. Co. Ltd (USA). EDC (1-ethyl-3-(3-dimethylaminopropyl) carbodiimide) and MES (4-morpholinoethanesulfonic acid) were obtained from the Tokyo Chemical Industry Co Ltd (JP), and NHS (*N*-hydroxysuccinimide) was attained from CovaChem LLC Company (US). Deionized water (18 MΩ cm) was acquired from an ultra-pure purification unit.

3.2. Instruments

The surface morphology of the as-prepared composite material was studied through Scanning Electron Microscopy (SEM) and elemental composition analysis using a Nova NanoSEM 450 field emission scanning electron microscope (FESEM) equipped with EDX. The crystallinity and phase structure of the composite were determined by X-ray diffraction (XRD) using a Rigaku-D/max-2500PC diffractometer at 40 kV with a graphite type monochromator working at 40 mA. The Fourier Transform Infrared (FTIR) spectroscopy measurements were recorded using a Thermo Fischer Scientific (Nicolet 6700, USA) spectrometer in the 600–4000 cm^{-1} scan range. The photoluminescence (PL) measurements of materials were obtained from a Xe lamp source F7000 Hitachi Spectrometer. Cyclic voltammetry was performed on an AMEL Electrochemistry Potentiostat (Model 2551) with a three-electrode system using an Ag/AgCl reference and platinum wire auxiliary electrode. The pencil graphite electrode (PGE) (diameter: 0.5 mm; length: 60 mm) was used as a working electrode acquired from Staedtler, Germany. Electrochemical impedance spectroscopy (EIS) was done on a 2700 Z-Pulse by AMEL Electrochemistry in the 0.1 Hz to 100 kHz range of frequency.

3.3. Synthesis of the $NiCr_2O_4$/g-C_3N_4 composite

Graphitic carbon nitride (g-C_3N_4) was synthesized in bulk using a previously described method.[21] The $NiCr_2O_4$/g-C_3N_4 composite was prepared by an *in situ* chemical reaction at ambient temperature. Typically, 1 g of $NaCr_2O_7$ and 2.5 g of Ni_2SO_4 were immersed in 100 mL of de-ionized water and ultrasonicated for 30 minutes. Then 5 g of g-C_3N_4 was added and stirred for 1 hour at room temperature. The prepared suspension was then stirred for another 2 hours and the precipitates were collected by centrifugation and washed with ethanol and water three times. The collected sample was dried at 60 °C for 24 hours and stored at room temperature.

3.4. Insects

Cultures of *T. castaneum* (Herbst) were reared in the laboratory under standard conditions. *A. mellifera* was collected from the honey bee collection centre of University of the Punjab and stored at −20 °C. *Z. nevadensis* was obtained from fallen logs and tree stumps from north Pakistan.

3.5. Preparation of AChE/Ni/GCN/PGE bioelectrodes

Three types of AChE/Ni/GCN/PGE biosensors were prepared differing in the source of AChE. The crude extracts were prepared using a previously described method.[21] The extracts were used directly as a source of insects' AChE. For electrode modification, the electrodes were electrochemically cleaned using 0.1 M H_2SO_4 and after washing with dH_2O and drying at RT, the functionalized Ni/GCN composite was adsorbed on the electrode surface by dipping in 2.5 μL of its aqueous suspension for 15 minutes. After drying and washing, the modified electrodes were immersed in 0.05 mL of AChE/EDC/NHS/MES extracts of *T. castaneum*, *A. mellifera* and *Z. nevadensis* in separate Eppendorf tubes for 15 minutes to allow for enzyme immobilization. The modified electrodes were then removed, dried at room temperature and washed carefully with deionized water to remove any unbound enzyme and impurities. The fabricated bioelectrodes were again dried and used for electrochemical measurements. The bonding mechanism depends on the activation of the carboxyl group functionalized material by EDC/NHS coupled enzyme molecules to make amide bonds between the amino group of the enzyme and carboxyl group of the material. Fig. 1 provides a schematic illustration of steps involved in fabrication of the biosensor.

3.6. Electrochemical measurement procedure

The electrochemical behaviour of the material on the surface of the electrode was determined through cyclic voltammetry using ferro-ferricyanide electrolyte solution at a potential ranging from −0.8 to +0.8 V. Similarly, the electro-catalytic ability of as-prepared biosensors was analysed through cyclic voltammetry using 0.1 M pH 7.4 PBS buffer electrolyte solution comprising acetylthiocholine chloride (ATCl), at a potential ranging from 0.2 to 0.9 V and 50 mV s^{-1} scan rate. The response of bare electrodes and modified controls was recorded and compared by observing the oxidation peak potential of Tch.

For enzyme inhibition by the pesticide, the modified electrodes were pre-incubated with malathion. The optimum inhibition time was determined by incubating the electrodes with malathion solution for 5 to 60 minutes, and 30 min was selected

as the optimum incubation time for malathion. CV was recorded afterwards, and percentage inhibition was calculated from the following formula:

$$[\%\ \text{Inhibition} = I^1 - I^0/I^1 \times 100]$$

where I^1 is the oxidation peak current of the control and I^0 is the oxidation peak current of the test in the presence of malathion. The calibration curves for each biosensor were generated using different concentrations of malathion and LOD was calculated for each.

3.7. Detection of malathion in wheat flour

The prepared biosensors were employed to detect malathion in whole wheat flour as a real sample using the procedure described previously.[21] The pesticide was spiked in 2 grams of wheat flour to obtain three concentrations covering the whole range, and the pesticide was extracted in acetonitrile : PBS (6 : 4 v/v) extraction solvent. After 10 minutes of incubation and centrifugation, the resulting supernatant was used as a pesticide mother solution to determine the percentage recovery of the pesticide using the same measurement procedure described above. The obtained results have been compared with a standard HPLC method using procedure as described in ref. 21.

3.8. Ligand and protein structure preparation

The structure for ligand, malathion in SDF format (CID: 4004) was obtained from PubChem (**https://pubchem.ncbi.nlm.nih.gov**). The homology models for Am-AChE (*A. mellifera*), Tc-AChE (*T. castaneum*), and Zn-AChE (*Z. nevadensis*) were built using YASARA (Yet Another Scientific Artificial Reality Application) Structure version 20.1.18 (ref. 21 and 71) and further refined by loop region optimization and steepest descent, simulated annealing minimization. The homology models for Tc-AChE, Am-AChE1, and Zn-AChE were obtained. Models were validated by YASARA z-scores, Ramachandran plot, PROCHECK server and VERIFY 3D showing acquisition of good quality homology modelled structures.

3.9. Molecular docking simulations

For Malathion molecular docking against three different AChE, YASARA Structure ver. 20.1.18 (ref. 71) with a modified AutoDock LGA algorithm and an AMBER03 force field was used.[21] For improved accuracy and better prediction of ligand–protein interactions, 100 global docking runs were obtained, rescored, and analyzed for dissociation constants, binding energy calculations and active site mapping as described in ref. 21. PyMol, Maestro, and PLIP were used to map the ligand–protein interactions.

4. Conclusions

In conclusion, the proposed work utilized the electrochemical biosensing approach to compare the malathion sensitivity based on three different insect and pest AChE enzymes that were immobilized on a potential $NiCr_2O_4$/g-C_3N_4 composite material. The surface and electrochemical properties of $NiCr_2O_4$/g-C_3N_4 favoured the immobilization and electrocatalytic activity of insects' enzyme, thus amplifying the sensitivity and amperometric response of the developed biosensors. The results suggested that the composite provides a biocompatible environment and potential binding sites for enzyme immobilization, a large surface area and high electrical conductivity, which resulted in good electrochemical performance of electrodes. The proposed platform was expected to be utilized to determine the sensitivity of OP insecticides and evaluate their toxicity against insects. Among three insect species, *A. mellifera* AChE was found to be immobilized with the highest efficiency and kinetic analysis showed its high affinity for the substrate. The electrocatalytic behavior of Am-AChE was also better than that of Tc-AChE and Zn-AChE; however, the malathion inhibition was observed at high concentrations compared to Tc-AChE and Zn-AChE, which showed that Tc-AChE and Zn-AChE are more sensitive to malathion than Am-AChE. The results were further confirmed through computational docking and the binding interactions of malathion with AChE of these insects were explored. These initial studies have opened ways for the rational designs of electrochemical biosensors and their use in the study of the insecticides' toxicity to insects. This study provides new development in the biosensor design, which offers considerable promise in several agriculture and environmental applications.

Author contributions

Sehrish Bilal: data curation, writing original draft, software, reviewing and editing; Muhammad Nasir: methodology, resources, and investigation; M. Mudassir Hassan: data curation and software; Muhammad Fayyaz ur Rehman: computational studies; Amtul Jamil Sami: supervision, methodology, investigation, and validation; Akhtar Hayat: supervision, methodology, resources, investigation, and validation.

Conflicts of interest

There are no conflicts to declare.

Acknowledgements

The authors acknowledge Pakistan Science Foundation for providing research grant to carry out this study under project PSF-MSRTII/AGR/P-COMSATS-LHR (09)/2019.

References

1 N. Gallai, J.-M. Salles, J. Settele and B. E. Vaissière, *Ecol. Econ.*, 2009, **68**, 810–821.
2 N. W. Calderone, *PLoS One*, 2012, **7**, e37235.
3 F. Sánchez-Bayo, D. Goulson, F. Pennacchio, F. Nazzi, K. Goka and N. Desneux, *Enviorn. Int.*, 2016, **89**, 7–11.
4 A. J. Sami, S. Bilal, M. Khalid, M. T. Nazir and A. Shakoori, *Pak. J. Zool.*, 2018, **50**, 725–733.
5 S. B. Walsh, T. A. Dolden, G. D. Moores, M. Kristensen, T. Lewis, A. L. Devonshire and M. S. Williamson, *Biochem. J.*, 2001, **359**, 175–181.

6 K. L. Newhart, *Environmentalfate of Malathion*, California Environmental Protection Agency, 2006, pp. 1–20.
7 N. E. Gary and E. C. Mussen, *Environ. Entomol.*, 1984, **13**, 711–717.
8 E. A. Parkin, *J. Sci. Food Agric.*, 1958, **9**, 370–375.
9 R. K. Upadhyay, G. Jaiswal and S. Ahmad, *Acta Univ. Sapientiae, Agric. Environ.*, 2010, **2**, 58–79.
10 F. Bughio and R. J. Wilkins, *J. Stored Prod. Res.*, 2004, **40**, 65–75.
11 N. White and R. J. Bell, *J. Econ. Entomol.*, 1988, **81**, 381–386.
12 E. Haubruge, M. Amichot, A. Cuany, J.-B. Berge and L. Arnaud, *Insect Biochem. Mol. Biol.*, 2002, **32**, 1181–1190.
13 D. Yong, C. Liu, D. Yu and S. Dong, *Talanta*, 2011, **84**, 7–12.
14 S. Rodriguez-Mozaz, M. J. de Alda and D. Barceló, *Anal. Bioanal. Chem.*, 2006, **386**, 1025–1041.
15 A. J. Baeumner, *Anal. Bioanal. Chem.*, 2003, **377**, 434–445.
16 P. Walter, A. Pepłowski, D. Janczak and M. Jakubowska, *Microelectron. J.*, 2019, 120–126.
17 A. El-Moghazy, E. Soliman, H. Ibrahim, T. Noguer, J.-L. Marty and G. Istamboulie, *Food Chem.*, 2016, **203**, 73–78.
18 N. Chauhan, J. Narang and C. Pundir, *Biosens. Bioelectron.*, 2011, **29**, 82–88.
19 X. Liu, R. Sakthivel, W.-C. Liu, C.-W. Huang, J. Li, C. Xu, Y. Wu, L. Song, W. He and R.-J. Chung, *Food Chem.*, 2020, 126889.
20 S. Liu, Z. Zheng and X. Li, *Bioanal. Chem.*, 2013, **405**, 63–90.
21 S. Bilal, M. M. Hassan, M. F. ur Rehman, M. Nasir, A. J. Sami and A. Hayat, *Food Chem.*, 2021, **346**, 128894.
22 J. Wang and E. Katz, *Anal. Bioanal. Chem.*, 2010, **398**, 1591–1603.
23 X. Zhu, L. Fan, S. Wang, C. Lei, Y. Huang, Z. Nie and S. Yao, *Anal. Chem.*, 2018, **90**, 6742–6748.
24 J. Xie, D. Cheng, P. Li, Z. Xu, X. Zhu, Y. Zhang, H. Li, X. Liu, M. Liu and S. Yao, *ACS Appl. Nano Mater.*, 2021, **4**, 4853–4862.
25 S. Zhang, R. Li, X. Liu, L. Yang, Q. Lu, M. Liu, H. Li, Y. Zhang and S. Yao, *Biosens. Bioelectron.*, 2017, **92**, 457–464.
26 G. T. Anand, L. J. Kennedy and J. J. Vijaya, *J. Alloys Compd.*, 2013, **581**, 558–566.
27 L. Shen, Q. Che, H. Li and X. Zhang, *Adv. Funct. Mater.*, 2014, **24**, 2630–2637.
28 N.-H. Li, Y.-H. Chen, C.-Y. Hu, C.-H. Hsieh and S.-L. Lo, *J. Hazard. Mater.*, 2011, **198**, 356–361.
29 S. A. Bakar, N. Soltani, W. M. M. Yunus, E. Saion and A. Bahrami, *Solid State Commun.*, 2014, **192**, 15–19.
30 A. K. Geim and K. S. Novoselov, in *Nanoscience and technology: a collection of reviews from nature journals*, World Scientific, 2010, pp. 11–19.
31 Z. Zhao, Y. Sun and F. Dong, *Nanoscale*, 2015, **7**, 15–37.
32 A. I. Cooper and M. J. J. Bojdys, *Mater. Today*, 2014, **17**, 468–469.
33 Y. Liu, M. Huang, J. Zhao, M. Lu, X. Zhou, Q. Lin, P. Wang and J. Zhu, *J. Electrochem. Soc.*, 2020, **167**, 066520.
34 S. Zhuiykov, T. Nakano, A. Kunimoto, N. Yamazoe and N. Miura, *Electrochem. Commun.*, 2001, **3**, 97–101.
35 H. Gao, J. Guo, Y. Li, C. Xie, X. Li, L. Liu, Y. Chen, P. Sun, F. Liu and X. Yan, *Sens. Actuators, B*, 2019, **284**, 305–315.
36 J. Tang, S. Ni, Q. Chen, X. Yang and L. Zhang, *J. Alloys Compd.*, 2017, **698**, 121–127.
37 L. P. Martin, A.-Q. Pham and R. S. Glass, *MRS Online Proc. Libr.*, 2002, **756**, 113.
38 M. Sabri, A. Habibi-Yangjeh and A. Khataee, *Chemosphere*, 2022, 134594.
39 R. Shafique, A. Mahmood, K. Batool, A. Ahmad, T. Yaqoob, M. Jabeen, A. U. Shah, U. Asjad and M. Rani, *ECS J. Solid State Sci. Technol.*, 2021, **10**, 101005.
40 R. Shafique, M. Rani, A. Mahmood, S. Khan, N. Janjua, M. Sattar, K. Batool and T. Yaqoob, *Int. J. Enviorn. Sci. Technol.*, 2021, 1–10.
41 R. S. Prakasham, G. S. Devi, C. S. Rao, V. Sivakumar, T. Sathish and P. Sarma, *Appl. Biochem. Biotechnol.*, 2010, **160**, 1888–1895.
42 H. Wang, W. He, X. Dong, H. Wang and F. Dong, *Sci. Bull.*, 2018, **63**, 117–125.
43 S. A. Shobeiri, M. Mousavi-Kamazani and F. Beshkar, *J. Mater. Sci.: Mater. Electron.*, 2017, **28**, 8108–8115.
44 L. Huang, H. Xu, Y. Li, H. Li, X. Cheng, J. Xia, Y. Xu and G. Cai, *Dalton Trans.*, 2013, **42**, 8606–8616.
45 X. Han, D. Xu, L. An, C. Hou, Y. Li, Q. Zhang and H. Wang, *Int. J. Hydrogen Energy*, 2018, **43**, 4845–4855.
46 S. Yang, Y. Gong, J. Zhang, L. Zhan, L. Ma, Z. Fang, R. Vajtai, X. Wang and P. M. Ajayan, *Adv. Mater.*, 2013, **25**, 2452–2456.
47 Y. Che, B. Lu, Q. Qi, H. Chang, J. Zhai, K. Wang and Z. Liu, *Sci. Rep.*, 2018, **8**, 1–12.
48 J.-y. Tang, R.-t. Guo, W.-g. Zhou, C.-y. Huang and W.-g. Pan, *Appl. Catal. B*, 2018, **237**, 802–810.
49 I. Papailias, T. Giannakopoulou, N. Todorova, D. Demotikali, T. Vaimakis and C. Trapalis, *Appl. Surf. Sci.*, 2015, **358**, 278–286.
50 S. Sun, E. Fan, H. Xu, W. Cao, G. Shao, B. Fan, H. Wang and R. Zhang, *Nanotechnology*, 2019, **30**, 315601.
51 B. Palanivel, C. Ayappan, V. Jayaraman, S. Chidambaram, R. Maheswaran and A. Mani, *Mater. Sci. Semicond. Process.*, 2019, **100**, 87–97.
52 T. Beenish, T. Muhammad and M. G. M. Nawawi, *Chem. Eng. Trans.*, 2021, **83**, 247–252.
53 B. Wang, Y. Li, H. Hu, W. Shu, L. Yang and J. Zhang, *PLoS One*, 2020, **15**, e0231981.
54 Y. Yang, Y. Zhao, F. Sun, T. You, Y. Gao and P. Yin, *Microchem. J.*, 2020, **159**, 105427.
55 X. Lu, L. Tao, Y. Li, H. Huang and F. Gao, *Sens. Actuators, B*, 2019, **284**, 103–109.
56 M. Kesik, F. E. Kanik, J. Turan, M. Kolb, S. Timur, M. Bahadir and L. Toppare, *Sens. Actuators, B*, 2014, **205**, 39–49.
57 Y. Al Naggar, G. Codling, A. Vogt, E. Naiem, M. Mona, A. Seif and J. P. Giesy, *Ecotoxicol. Enviorn. Saf.*, 2015, **114**, 1–8.
58 V. Bommuraj, Y. Chen, M. Birenboim, S. Barel and J. A. Shimshoni, *Chemosphere*, 2021, **266**, 128974.
59 A. D. Noi, S. Casini, T. Campani, G. Cai and I. Caliani, *Int. J. Environ. Res. Public Health*, 2021, **18**, 1863.
60 A. J. Sami, S. Bilal, M. Khalid, M. T. Nazir and A. R. Shakoori, *Pak. J. Zool.*, 2018, **50**, 725–733.
61 B. M. Woldegebriel, *ECS Meeting Abstracts*, 2020.

62 C. S. Kushwaha and S. K. Shukla, *J. Mater. Sci.*, 2019, **54**, 10846–10855.
63 M. Guler, V. Turkoglu and A. Kivrak, *Environ. Sci. Pollut. Res.*, 2016, **23**, 12343–12351.
64 S. Ebrahim, R. El-Raey, A. Hefnawy, H. Ibrahim, M. Soliman and T. M. Abdel-Fattah, *Synth. Met.*, 2014, **190**, 13–19.
65 O. Yamauchi, A. Odani and M. Takani, *J. Chem. Soc., Dalton Trans.*, 2002, 3411–3421.
66 G. Faccio, *Sensors*, 2018, **18**, 1204.
67 K. Khaldi, S. Sam, A. Gouget-Laemmel, C. Henry de Villeneuve, A. Moraillon, F. Ozanam, J. Yang, A. Kermad, N. Ghellai and N. Gabouze, *Langmuir*, 2015, **31**, 8421–8428.
68 Y. H. Kim, D. J. Cha, J. W. Jung, H. W. Kwon and S. H. Lee, *PLoS One*, 2012, **7**, e48838.
69 A. J. Sami, S. Bilal, M. Khalid, F. R. Shakoori, F. Rehman and A. R. Shakoori, *Pak. J. Zool.*, 2016, **48**, 881–886.
70 M. A. Saleem and A. R. Shakoori, *Arch. Insect Biochem. Physiol.*, 1987, **5**, 45–55.
71 E. Krieger and G. Vriend, *Bioinformatics*, 2014, **30**, 2981–2982.